Supramolecular Structures in Aqueous Solutions of Rigid Polyelectrolytes with Monovalent and Divalent Counterions

Anja Kroeger,[†] Joerg Belack,[†] Antje Larsen,[‡] George Fytas,[†,‡] and Gerhard Wegner*,[†]

Max Planck Institute for Polymer Research, Ackermannweg 10, 55128 Mainz, Germany, and Department of Materials Science and Technology, University of Crete and F.O.R.T.H., P.O. Box 1527, 71110 Heraklion, Greece

Received June 2, 2006; Revised Manuscript Received August 4, 2006

ABSTRACT: Dodecyl-substituted poly(*p*-phenylene)sulfonates (PPPS), which are models of rodlike polyelectrolytes, form cylindrical micelles in aqueous solutions. The effect of different counterions on the association behavior of PPPS in water is investigated by isotropic and anisotropic dynamic light scattering. PPPS of $M_{W,p} = 21 \times 10^3$ g/mol forms micelles of a weight-average length of 600−700 nm and 15−20 individual chains per cross section in very dilute solution. The exact values are depending on whether H^+ or Na^+ serves as counterion and whether neutral salt is present or not. The form factor of the formed objects can be analyzed in terms of a weakly bending rod (Koyama's form factor). Micelles of the same polymer in the presence of Ca^{2+} or Ba^{2+} exhibit approximately the same length but have around 50 chains per cross section; they are interpreted as defined bundles of a few micelles exhibiting on average the shape of a weakly bending rod. The inferred structures are supported by images of transmission electron microscopy.

Introduction

Polyelectrolytes in aqueous environment are characterized by a complex pattern of long- and short-range interactions.[1,2] Short-range excluded volume and long-range electrostatic interactions composed of both intra- and intermolecular components contribute to the overall solution properties.[3−5] Moreover, the fact that highly mobile counterions and macroions are simultaneously present has a strong impact on the dynamics of polyelectrolyte solutions.[6] The combination and mutual interdependencies of these long-range and short-range interactions lead to self-organization phenomena[7−9] which are fundamental to the functioning of life in the case of certain classes of biogenic polyelectrolytes and are of importance to a number of applications of synthetic polyelectrolytes.

The key example for a biogenic class of charged polymers refers to the nucleic acids DNA and RNA.[10] In the case of DNA each repeat unit exhibits one ionogenic phosphate group. The formation of the double-stranded DNA from the single-stranded one is strongly influenced by the pH, ionic strength of the medium, and type of mobile counterion present. Supercoiling of the double-stranded DNA is again controlled by the presence of certain counterions, ionic strength, and temperature. Thus, self-organization is a function of the complex interdependence of the long-range forces, namely repulsion or screening of charged sites on the macromolecule in competition with short-range effects coming from excluded volume and van der Waals forces acting on the length scale of the chemical repeat unit of the chains.

Further examples among the biopolymers are proteoglycans as found in the connective tissues, in external matrices, and on the surface of many cells.[11] They all contain glycosaminoglycans defined as linear polymers of specific disaccharides. One of these sugar residues consists typically of uronic acid and at least one; frequently both of these residues are sulfatated. Thus, each of these polymer chains bears many fully ionized negative charges. These proteoglycans are thought to be essential in the recognition process, which leads to the anchoring of the cells to matrix fibers.[12] Similarly, many proteins contain ionogenic amino acid residues that provide a charge pattern along the chain which is frequently essential in the further self-organization to secondary, tertiary, and higher levels of structure.[13,14] The accurately defined topologies seen in the tertiary and quaternary protein structures are essential in the creation of areas of high and low charge density at the surface. The pattern thus created serves the purpose of molecular recognition through ionic interactions.[15]

The intramolecular interaction among far away segments of the same macromolecule, which is influenced by or will induce coiling and folding and thus will lead to particular shapes, is substantially influenced by the effect of counterion localization around the macroions.[16] This counterion condensation is also responsible for a large decrease of the effective total charge of the macroion. It contributes to an attraction between different parts of a flexible polymer chain by mutual polarization of the ion clouds localized around the chain segments, and this contributes to the overall conformation.[17,18] In other words, segments together with their ion clouds separated over a long distance along the chain trajectory may nevertheless interact dynamically mediated by the attractive forces which have their origin in the polarizability of the ion cloud. This has been pointed out first by Oosawa.[19] In contrast to this, conformationally rigid and rodlike polyelectrolytes remain in their extended chain conformation provided that their total length does not surpass their persistence length by a large factor.[20] Consequently, only intermolecular interactions determine the properties of such systems.[21,22] The interplay between excluded volume effects and long-range electrostatic interactions must lead to self-organization phenomena in such rodlike or wormlike polyelectrolytes. Since it is known that self-organization and molecular recognition phenomena in biogenic polyelectrolyte

[†] Max Planck Institute for Polymer Research.
[‡] University of Crete and F.O.R.T.H.
* Corresponding author. E-mail: wegner@mpip-mainz.mpg.de.

10.1021/ma061228v CCC: $33.50
Published on Web 09/12/2006

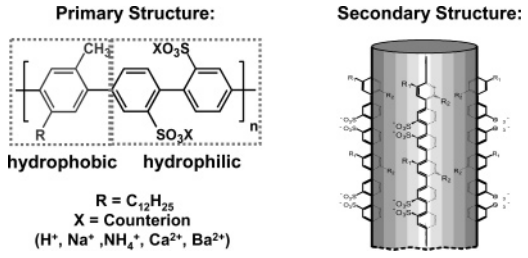

Figure 1. Primary structure of the alkyl-substituted sulfonated poly(*p*-phenylene) and a schematic picture of a section of a single cylindrical micelle (secondary structure). The hydrophobic and hydrophilic parts of the chemical repeat unit of the polymer are indicated in the primary structure.

systems are strongly modified by the nature, i.e., type and charge of the mobile counterions, as well as by the ion strength of the solution, one could expect that the same is true for structurally simpler synthetic model polyelectrolytes. The hope is that the reduced complexity of the chemical structure of the underlying synthetic macromolecules compared to the biogenic polyelectrolytes allows identifying the role of the individual parameters in hierarchical structure formation and concomitant recognition processes.

On this account Rulkens et al.[23] and Bockstaller et al.[24] have introduced a simplified model system, which allows performing systematic investigations. The primary structure of this model system consists of a conformationally rigid backbone composed of phenylene rings which are linked in the para position. Every third phenylene ring carries one methyl and one dodecyl side group while the two remaining phenylene rings carry each just one sulfonic acid residue. The latter provide the compatibility with water and are the ionogenic centers responsible for the polyelectrolyte behavior while the phenylene rings carrying the aliphatic side groups are hydrophobic in nature. The hydrophobic−hydrophilic balance which is thus embedded in the primary structure results in the strong tendency of these macromolecules to form a well-defined secondary structure in water. Previous work has shown that this secondary structure can be described as cylindrical micelles of a cross section, the dimension of which relates to the primary structure and allows defining a radial aggregation number, N_{rad}. It has further been shown that the micelles have a contour length much larger than the length of the constituent macromolecules. This could be characterized by an axial aggregation number, N_{ax}. The primary and secondary structures of this model system are shown in Figure 1. The cylindrical micelles are described by a bundle of poly(*p*-phenylene) chains oriented parallel to the cylinder axis with their dodecyl substituents pointing inward and the sulfonate residues making contact with the aqueous medium pointing outward. It is thus the underlying assumption which is well supported by previous measurements[25] that alkyl-substituted poly(*p*-phenylene)sulfonates (PPPS) behave as a kind of polysoap.[26] The formed micelles are rather stable objects, which undergo further interactions to form tertiary and even quaternary structures.[25,26] Even at the lowest examined concentration ($c_p \sim 8 \times 10^{-4}$ g/L), at which scattering experiments can be conducted, only micelles were identified, and hence the critical micelle concentration is immeasurably small.

Studies by Bockstaller et al.[24,25] on the sodium salt form of PPPS (PPPS-Na) revealed that the micelles are the single objects forming an isotropic solution up to a concentration of 0.02 g/L in water at 20 °C. These start to associate into aggregates composed of still a small number of micelles at a defined concentration, and these aggregates give rise to a gel phase at still higher concentration. Rulkens et al.[27] as well as Zaroslov et al.[28] have reported that under certain conditions of experimental parameters lyotropic liquid crystal phases of the micelles could be identified. However, the type of aggregate and nature of the lyotropic phase seem to depend[29] on the chain length of the primary macromolecules, the counterion species, and ionic strength of the solution.

The aim of the present study is, therefore, to elucidate the role of the specific counterions on the self-organization of these wormlike polyelectrolytes starting from carefully purified samples in the acid form (PPPS-H), where only protons in their hydrated form are present as mobile couterions. It may be noted in passing that PPPS is by its very nature a "strong" electrolyte, and thus, the system does not suffer from a pH dependence of ionization. Chlorides of mono- or divalent cations were added to the solution of the free polymer acid in a concentration comparable to the molar concentration of the polymer bound sulfonate residues. The effect of these ionic additives as seen by static and dynamic light scattering is the central issue of this paper. The effects seen by scattering techniques in dilute solution are supplemented by direct imaging via transmission electron microscopy of some of the aggregates whose structure can be inferred to by the interpretation of all scattering data.

Experimental Section

Materials. The synthesis of PPPS of the detailed structure shown in Figure 1 has been described in the literature.[23,27,30] In the present study two samples of the free acid form, PPPS-H21 and PPPS-H30, with weight-average molar mass $M_{W,p} = 21$ kg/mol and $M_{W,p} = 30$ kg/mol and similar polydispersity $M_{W,p}/M_{n,p} \approx 2$ were employed. The absence of ionic impurities had been certified by atomic absorption spectroscopy (AAS). A high concentration ($c_p = 0.34$ g/L) of PPPS-H was prepared by dissolving the sample in ultrapure water (Millipore, Milli-Q water with a conductivity < 18.2 MΩ·cm) under continuous stirring for several hours. Lower concentrations were prepared from this stock solution by dilution with ultrapure water. The desired ionic species in the aqueous solutions of PPPS-H were added in form of their chloride salts. Dust-free solutions for light scattering experiments were obtained by filtration through cellulose acetate membrane filters with a pore size of 0.45 μm (Millipore, Millex-HA) into silica glass light scattering cuvettes (Hellma, inner diameter = 20 mm), which were cleaned before with acetone in a Thurmont apparatus.[31] The concentration in the aqueous solution after filtration was also verified by UV spectroscopy.

Photon Correlation Spectroscopy (PCS). In a dynamic light scattering (DLS), the experimental normalized autocorrelation function $G(q,t) = \langle I(q,0)I(q,t)\rangle/\langle I(q)\rangle^2$ of the light scattering intensity $I(q)$ at a scattering vector $q = (4\pi n/\lambda_0)\sin(\theta/2)$ (n is the refractive index, θ denotes the scattering angle, and λ_0 is the wavelength of the incident laser beam) is related to the normalized time correlation function $g(q,t) = \langle E^*(q,0)\,E(q,t)\rangle/\langle|E(q,0)|^2\rangle$ of the scattered electric field $E(q,t)$ by the Siegert relation

$$G(q,t) = 1 + f^*|\alpha g(q,t)|^2 = 1 + f^*|C(q,t)|^2 \qquad (1)$$

where f^* is a coherence instrumental factor and α is the fraction of the total scattered intensity $I(q)$ associated with fluctuations relaxing with times longer than 0.1 ms.[25,32] To analyze the computed relaxation functions $C(q,t)$, an inverse Laplace transformation using the constraint regularized CONTIN method was applied.[33] This method assumes that $C(q,t)$can be written by a superposition of exponentials

$$C(q,t) = \int_{-\infty}^{\infty} H_\tau(\ln\tau)\exp[-t/\tau]\,\mathrm{d}(\ln\tau) \qquad (2)$$

where $H_\tau(\ln\tau)$ is the distribution of relaxation times. The characteristic relaxation times correspond to the peak positions of

$H_\tau(\ln \tau)$, and the area under the peak defines the value α (eq 1) and hence the intensity $\alpha I(q)$ associated with the particular dynamic process. For single but nonexponential decay, $C(q,t)$ can be represented by the stretched exponential Kohlrausch−Williams−Watts (KWW) function

$$C(q,t) = \alpha \exp[-(t/\tau^*(q))^{\beta}] \quad (3)$$

where the shape parameter $0 < \beta \leq 1$ characterizes the distribution of relaxation times.[32]

The experiments were performed on a commercial goniometer from ALV equipped with a krypton ion laser (Spectra Physics model 2020 with a single mode intensity of 100 mW at $\lambda = 647.1$ nm) and a Nd:YAG dye-pumped, air-cooled laser (Adlas DPY 325 with a single mode intensity of about 50 mW at $\lambda = 532$ nm) by using an ALV-5000 full digital correlator (320 channels) over a time range $10^{-7} \leq t \leq 10^3$ s. The cuvettes containing the solutions were placed into a thermostated refractive index matching toluene bath held at a constant temperature of $T = 20$ °C. For all light scattering experiments, the primary laser beam and the scattered light passed through Glan-Thomson polarizers with an extinction coefficient better than 10^{-7}. The first polarizer guarantees that only vertically (V) polarized light meets the sample. For the depolarized dynamic light scattering measurements, the analyzer was changed from vertical (VV) to horizontal (VH) position with respect to the scattering plane. Static light scattering experiments were performed with the same instrumental setup and equipment over an angular range from 12° to 150° corresponding to $q = 3.29 \times 10^{-3}$−3.04×10^{-2} nm^{-1} (for $n = 1.33$) at room temperature $T = 20$ °C. The reduced absolute intensity ratio $R(q)/(Kc)$ at a concentration c is computed from the Rayleigh ratio $R(q)$

$$R(q) = \frac{I(q)_{soln} - I(q)_{solv}}{I(q)_t}\left(\frac{n_{solv}}{n_t}\right)^2 R_t \quad (4)$$

and the optical constant $K = (2\pi n\, dn/dc)^2/(\lambda_0^4 N_A)$; I_{soln}, I_{solv}, and I_t are respectively the light scattering intensities of the solution, solvent, and the pure toluene used as a standard with refractive index n_t and Rayleigh ratio $R_t = 2.2 \times 10^{-5}$ cm^{-1} whereas N_A is the Avogadro number.[34] The refractive index increment dn/dc (∼0.189 mL/g) for each sample of PPPS was measured at $\lambda = 633$ nm using a scanning Michelson interferometer.[35]

Transmission Electron Microscopy (TEM). A Tecnai F20 transmission electron microscope from FEI Co. with integrated electron energy-loss spectrometer, operated at a 200 kV acceleration voltage, was used for recording of the cryo-TEM images of the specimens. For cryofixation of the samples, the aqueous solution was dropped onto a gold-stabilized carbon grid, and the excess amount of liquid was blotted off with filter paper. Subsequently, the sample was frozen in liquid propane (−85 °C) and transferred to the TEM.

Results and Discussion

Structure of the Assemblies. a. Monovalent Counterions. In the case of the sodium salt of PPPS, the dilute aqueous solutions consist of cylindrical micelles of the form depicted in Figure 1. Individual macromolecules could not be detected even at a concentration as low as $c_p = 8 \times 10^{-4}$ g/L. For PPPS-Na, the radial aggregation number was found[26] to be $N_{rad} \sim 15$ independent of the molar mass of the primary macromolecules. Here, we are interested in the structures in the aqueous solution of the free acid form of PPPS. A sample of weight-average molar mass $M_{W,p}$ of 21 kg/mol of the primary macromolecules was dissolved in ultrapure water and studied under salt-free conditions by light scattering. Figure 2 shows the concentration dependence of the reduced total scattered intensity $Kc/R_{VV}(q \rightarrow 0)$ for PPPS-H21 in the range $8 \times 10^{-4} \leq c_p \leq 0.1$ g/L. This plot suggests two different regimes with a crossover concentration $c_{crit} = 0.012$ g/L. In the regime A only single supramolecular objects (micelles) were documented, and intermolecular interactions between these micelles should not play a significant role. The structural characterization and the investigation of dynamic behavior of individual micelles in the presence of different counterions refer to this regime. To minimize intermolecular interaction effects, very dilute solutions with a polymer concentration $c_p = 3.4 \times 10^{-3}$ g/L are used for the structural characterizations.

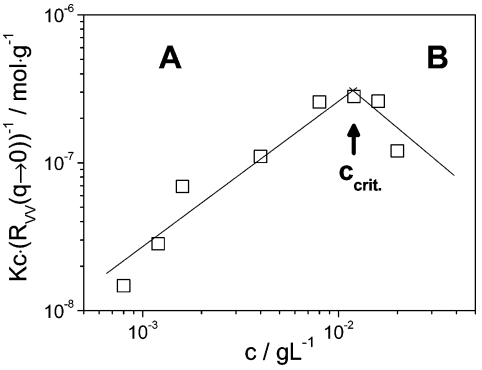

Figure 2. Concentration dependence of the reciprocal total static scattering intensity $Kc/R_{VV}(q \rightarrow 0)$ as a function of polymer concentration c_p of aqueous solutions of PPPS-H21 at 20 °C. At $c_{crit} \cong 0.012$ g/L, a crossover occurs from regime A in which individual micelles exist to a regime B in which aggregates of the micelles are found.

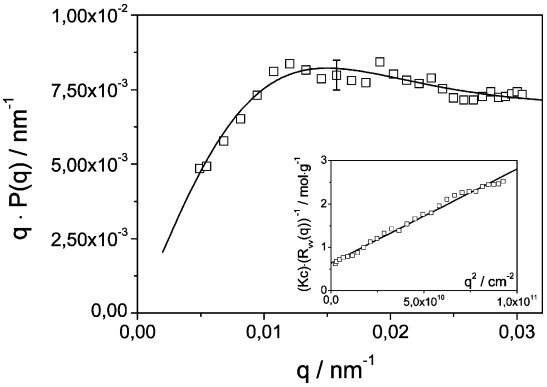

Figure 3. Holtzer plot of the static light scattering intensity of PPPS-H21 in salt-free solution at $c_p = 3.4 \times 10^{-3}$ g/L. The solid line denotes the form factor of a nearly rigid rod of length $L = 600$ nm according to eqs 5 and A1 with size polydispersity, PD = 3. The inset shows the plot of $Kc/R_{VV}(q)$ vs q^2 for the determination of the molar mass and the radius of gyration of the micellar rod.

The first target is the shape and the dimensions of the micelles of PPPS-H21. Figure 3 shows a Holtzer presentation of the form factor $P(q) = R_{VV}(q)/(M_W/Kc)$ of PPPS-H21 in a salt-free aqueous solution as a function of the scattering vector q. The weight-average molar mass M_W of the supramolecular assembly is obtained from the $Kc/R_{VV}(q)$ vs q^2 plot in the linear regime, as shown in the inset of Figure 3. The intercept and the slope of this plot respectively yields $M_W = (4 \pm 0.5) \times 10^6$ g/mol and the radius of gyration $R_G = 144 \pm 9$ nm, as listed in Table 1. On the basis of the form of the experimental $qP(q)$, which increases at low q values and reaches a quasi-plateau in the high q range, we conclude that the whole object is probed. Thus, the experimental conditions justify the unambiguous report of the M_W and the estimation of the overall size $2\pi/q_m \sim 500$ nm from the value of q_m at which $qP(q)$ exhibits its maximum. The plateau value allows estimating the linear mass density $M/L = qR_{VV}(q)/(cK\pi)$ listed in Table 1. The solid line in Figure 3 denotes the Koyama form factor[36−39]

$$P_{\text{Koyama}}(L_r, ql_k) = \frac{2}{L_r^2}\int_0^{L_r}(L_r - x)\exp\left[-\frac{1}{3}s^2 x f(x)\right]\frac{\sin(sxg(x))}{sxg(x)}\,dx \quad (5)$$

which considers a weakly bending rod of length $L = 600$ nm with a size polydispersity PD = 3 ($L_r = L/l_k$, $s = ql_k/2$, see Appendix A; note that the derivation of this form factor found in the literature[36−39] is difficult to reproduce, and therefore we have given a lucid derivation in the Appendix).

Furthermore, the TEM micrograph of Figure 4 supports the found structure of long and thin cylindrical micelles. However, a correct estimation of their length distribution is hampered by the relatively small number of observed micelles per drop of the PPPS-H21 solution in the cryofixation experiment. A single highly anisotropic object with short branches is seen in Figure 4. Statistical analysis of many such cryo-TEM micrographs by using the software program ImageJ results in an average diameter $d = 5 \pm 1$ nm and a length of $L_\varnothing = 515 \pm 52$ nm, in conformity to the light scattering data (Table 1). We note that the experimental form factor is not sensitive to the value of d due to the low magnification of the light scattering experiment, i.e., $qd \ll 1$. However, the density distribution across the diameter of the micelles can in principle be determined from small-angle X-ray scattering (SAXS) data, and in fact, such an analysis has been performed for our systems (sodium salt of PPPS) by Bockstaller et al.[25] The pertinent result was that the density in the center of the micelle is lower than that at the rim, probably indicating that the micelle is swollen by water.

Sodium chloride was then added to this solution of PPPS-H21 at a sodium chloride (NaCl) concentration $c_{NaCl} = 4.74 \times 10^{-5}$ mol/L, at which the nominal concentration of sodium ions is 4 times larger than the concentration of sulfonic acid residues fixed to the polymer backbone. The light scattering intensity obtained from both static and DLS experiments is depicted in a Holtzer presentation in Figure 5. The displayed similarity between PPPS-H21 and PPPS-Na21 intensity patterns suggests that the structure of the micelles remains largely unaffected by the addition of NaCl. The same data analysis as for the free acid of PPPS reveals that the number of chains per cross section of the cylindrical micelles $N_{rad} = M_W L_m/(M_m L_W)$ with $M_m = 571$ g/mol and $L_m = 1.2$ nm being the molar mass and the length of the monomer unit grows by ca. 30% as reflected in a similar increase in the linear mass density (M/L) of the objects. At the same time the contour length $L_W = M_W/(M/L)$ decreases by ca. 10% while the total mass of the objects increase by ca. 20%. The radius of gyration $R_G \sim 150$ nm remains virtually unchanged. This assembly remains stable at ambient temperature up to 0.1 g/L. In the semidilute regime, the system becomes unstable as it was also observed in the aqueous solutions of sodium polystyrenesulfonate.[40] It should be mentioned that amphiphilic short poly(*p*-phenylenes)[41] in surfactant solutions form also rodlike micelles with $N_{rad} \sim 15$.

b. Divalent Counterions. The effect of the presence of divalent counterions for the self-organization of PPPS-H was studied using calcium chloride and barium chloride as the additive to the aqueous solution at $c_p = 3.4 \times 10^{-3}$ g/L. The excess of divalent counterions with regard to the sulfonate residues was adjusted by the concentration of the added salt at 4.74 $\times 10^{-5}$ mol/L. Incubation of the aqueous solution of PPPS-H21 with the salts of the divalent counterions was witnessed by a strong increase of the light scattering intensity at low q, which has reached a constant level after about 12 h. No noticeable change was observed for several months keeping the solutions at ambient temperature.

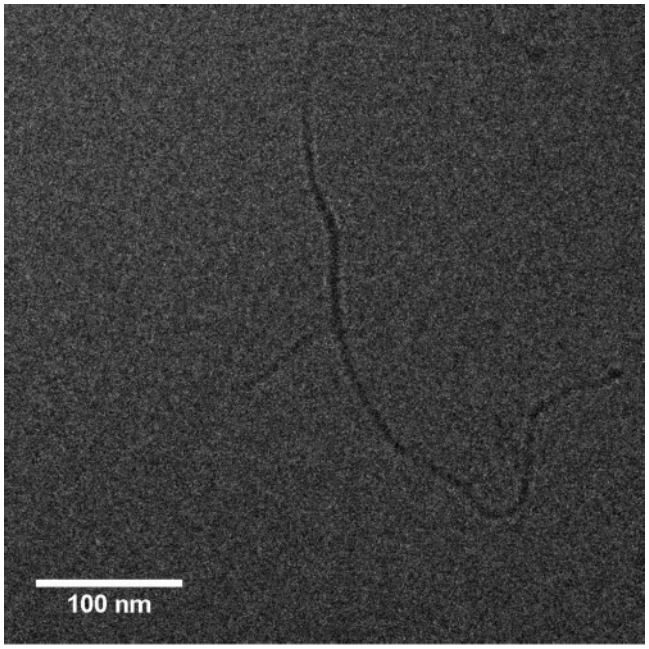

Figure 4. Transmission electron microscopy (TEM) image of a micelle of PPP-H21 in dilute salt-free aqueous solution at $c_p = 3.4 \times 10^{-3}$ g/L obtained by cryofixation.

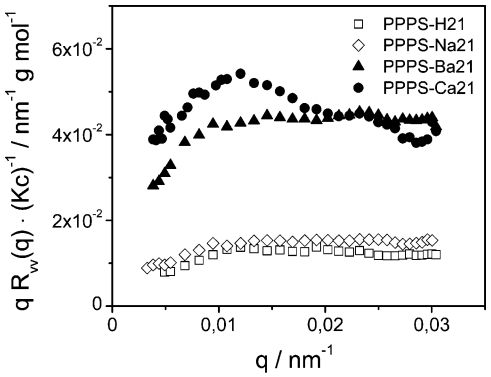

Figure 5. Absolute light scattering intensity for several dilute solutions of PPPS-H21 at $c_p = 3.4 \times 10^{-3}$ g/L without and with added salt of $c_{salt} = 4.74 \times 10^{-5}$ mol/L in a Holtzer presentation. Open squares and diamonds denote experimental data for "salt-free" PPPS-H21 and NaCl added PPPS-Na21 samples, whereas the solid triangles and circles refer to samples PPPS-Ba21 and PPPS-Ca21 with added $BaCl_2$ and $CaCl_2$ salts.

The measured intensity distribution $I(q)$ for the two divalent solutions is also shown in Figure 5 for comparison purposes. The light scattering intensity increases in comparison to the salt-free solution substantially which suggests an increase for both the molar mass $M_W \sim (15-19) \times 10^6$ g/mol and the radial aggregation number $N_{rad} \sim 50$ of the formed objects. The relevant structural parameters extracted from the scattering patterns

Table 1. Characteristics of the Micelles of PPPS-H21 under Salt-Free Conditions and with NaCl Added ($c_p = 3.4 \times 10^{-3}$ g/L and $c_{NaCl} = 4.74 \times 10^{-5}$ mol/L)

counterion	$M_W/10^6$ g/mol	L_W/nm	R_G/nm	N_{rad}	M/L 10^3 (g/mol) nm^{-1}
H^+	4.0 ± 0.5	560 ± 30	144 ± 9	14 ± 3	7.2 ± 0.8
Na^+	4.8 ± 0.4	490 ± 25	146 ± 9	19 ± 4	9.8 ± 1

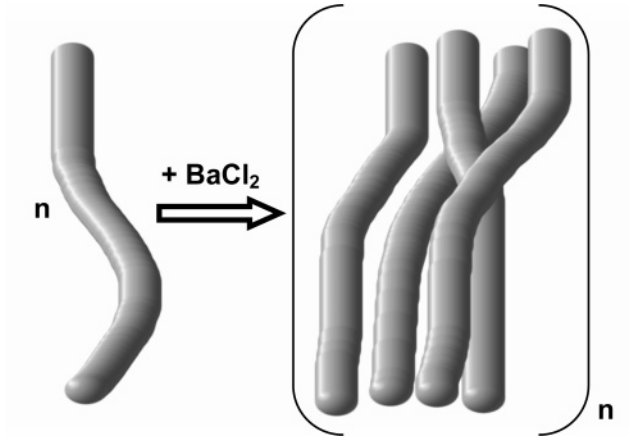

Figure 6. Schematic picture of a counterion induced side-by-side aggregation of the original objects onto a bundle of individual micelles.

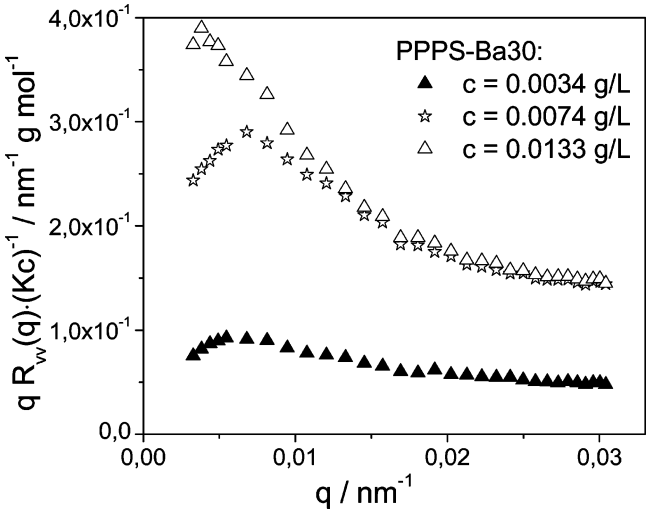

Figure 7. Absolute light scattering intensity patterns for PPPS-Ba30 at three different PPPS-H30 concentrations with $BaCl_2$ being present in 4-fold excess.

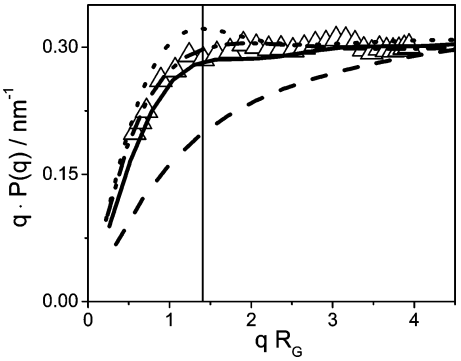

Figure 8. Form factor $P(q)$ for PPPS-Ba21 in aqueous solution with $c_p = 3.4 \times 10^{-3}$ g/L at 20 °C in a reduced Holtzer presentation. The lines denote theoretical representations of the data (triangles) by monodisperse (solid line), polydisperse (dashed line) rigid rods, and Koyama-type semiflexible monodisperse (dotted line) and polydisperse (dash−dotted line) rods. The vertical line at $qR_G = 1.4$ marks the position at which $qP(q)$ attains its maximum for monodisperse rods.[32]

are compiled in Table 2. The peak at low q values implies the presence of structures with large dimensions of the order of few hundred nanometers. The appearance of the peak in the experimental q range further suggests that despite the large structures involved, the low light scattering q values can still match the overall size of the probed object, which appears to be counterion specific.

A comparison of the data in Tables 1 and 2 indicates that the addition of the divalent ions causes a nearly 4−5-fold increase in the mass of the scattering objects. This increase in mass owes its origin mainly to a respective increase in N_{rad} as inferred from the increase in the mass per unit length M/L (Figure 5, plateau at high q values), while the contour length L_W and R_G remain rather unchanged. Since the cross section of the original micelles of PPPS-H21 is rather fixed by the hydrophobic−hydrophilic balance embedded in the chemical structure of the repeat unit, these data seem to imply that new objects are formed by counterion-induced side-by-side aggregation of the original objects onto bundles of an average but not too large number of individual micelles, as illustrated in Figure 6. We cannot dispute, however, that the enhanced light scattering intensity in the presence of divalent salts might hint to an enclosed phase separation since the second virial coefficient remains negative. Theoretically,[42] the presence of multivalent salts can enhanced incompatibility of highly charged polyelectrolyte solution due to increased segment−segment attraction.

To probe this conjecture, we have examined the variation of the scattering intensity pattern with concentration. By concentrating an aqueous solution of the PPPS-H30 at a initial concentration of 3.4×10^{-3} g/L and $BaCl_2$ concentration of 4.74×10^{-5} mol/L (PPPS-Ba30), we examined the variation of the scattering intensity with concentration in the range $3.4 \times 10^{-3} \leq c_p \leq 1.33 \times 10^{-2}$ g/L depicted in Figure 7. The concentration dependence of $I(q)/c_p$ at low q values leads to a negative second osmotic virial coefficient of $A_2 = -5 \times 10^{-4}$ mol ml g^{-2}. While nonfavorable interactions are present, the A_2 value is low, and therefore the increase of $I(q)$ with increasing c_p should rather imply an increasing size of the formed aggregates and not enhanced concentration fluctuations near to phase separation. To elucidate these structures in dilute aqueous solutions of PPPS in the presence of divalent salt, we have chosen the PPPS-Ba21 solution at $c_p = 3.4 \times 10^{-3}$ g/L.

Figure 8 shows the experimental form factor $P(q)$ as a function of the reduced quantity qR_G. To create this plot, the required weight-averaged molar mass $M_W = (15 \pm 1) \times 10^6$ g/mol and the radius of gyration $R_G = 160 \pm 8$ nm were obtained from the intercept and the slope of the Kc/R_{VV} (q) vs q^2 at low q values as delineated above (cf. Figure 3). The description of the experimental form factor should include size polydispersity in the theoretical[41] $P(q)$ as inferred from the nonexponential shape of the relaxation functions for the concentration and orientation fluctuations (see below).

Table 2. Characteristics of the Self-Assembled Structures in the Aqueous Solution of PPPS-Ca21 and PPPS-Ba21, Obtained by Starting from PPPS-H21 ($c_p = 3.4 \times 10^{-3}$ g/L) Followed by Addition of $CaCl_2$ and $BaCl_2$ ($c_{salt} = 4.74 \times 10^{-5}$ mol/L)

	DLS		SLS				
counterion	D_z/cm^2 s^{-1}	L_z/nm	$M_W/10^6$ g/mol	L_W[a]/nm	R_G/nm	N_{rad}	M/L 10^3 (g/mol) nm^{-1}
Ca^{2+}	2.5×10^{-8}	870 ± 40	19 ± 1.4	680 ± 35	160 ± 8	52 ± 5	28 ± 2.5
Ba^{2+}	3.0×10^{-8}	725 ± 35	15 ± 1.3	570 ± 30	161 ± 8	51 ± 5	27 ± 2.4

[a] $L_W = M_W/(M/L)$.

$$P_z(q,L,W) = \frac{\int_0^\infty P(q)\, W(L) L \, dL}{\int_0^\infty W(L) L \, dL} \quad (6)$$

where $W(L)$ denotes the distribution of contour lengths L assuming to be of a Schulz−Zimm type

$$W(L) = \frac{L^m}{m!} y^{m+1} e^{-yL} \quad (7)$$

with $y = (m + 1)/L_W$, where m is a parameter characterizing the polydispersity of the structures $[m^{-1} = (L_W/L_{n-1})]$.[43] For the form factor $P(q)$ of PPPS-Ba21, we assume first a rigid-rod shape[44]

$$P_{rod}(q) = \frac{2}{qL}\int_0^{qL} \frac{\sin x}{x} dx - \left(\frac{\sin(qL/2)}{qL/2}\right)^2 \quad (8)$$

with $L_W = R_G\sqrt{12} = 450$ nm and a negligible diameter. A polydispersity PD = 1 leads to the solid line in Figure 8, whereas introduction of a PD = 3 (dashed line) with $L = 300$ nm worsens the fit significantly.[43] An alternative approximation to a semiflexible structure approached from the rigid-rod limit was proposed by Koyama.[36−39] Although this form factor has been rarely utilized,[37−39] we employ it to represent the experimental $P(q)$ mainly because of the resemblance of the present structures more to rod rather than to coil conformations. The dotted line in Figure 8 denotes the Koyama form factor (eq 5) for monodisperse structures with $L = 750$ nm and Kuhn segment length $l_k = 750$ nm which capture the experimental R_G. The computed $P(q)$ displays deviations from the experimental data in the $1 < qR_G < 2$ range. Inclusion of size polydispersity (see Appendix A) into the Koyama form factor (eq 5) with PD = 3, $L = 750$ nm, and $l_k = 400$ nm clearly leads to a better representation of the experiment (dashed−dotted line in Figure 8). We should note that both models suggest almost micrometer-sized supramacromolecular structures which should also manifest themselves in the transport properties, namely translational D_z and rotational D_R diffusion coefficients. Hence, a consistent description of both static and dynamic properties will add credibility to the proposed size and shape of these association colloidal objects.

Figure 9 displays the relaxation function $C(q,t)$ (eq 1) for the PPPS-Ba21 system at low and high magnification corresponding to $qR_G = 0.53$ and 3.95. We first assume one single translational diffusion mechanism for the decay of the concentration fluctuations in the dilute solution of these polydisperse objects.[32,41]

$$C(q,L,t) = \frac{\int_0^\infty P(qL) L W(L) e^{-D_z q^2 t} \, dL}{\int_0^\infty L W(L) \, dL} \quad (9)$$

At low q values, eq 9 adequately describes the experimental $C(q,t)$ as shown by the solid line in Figure 9. Because of the domination of the scattering at low q values by the large objects, the moderate width of the $C(q,t)$ is also described by eq 3 with $\beta = 0.9$. At the highest q, eq 9 predicts (solid line in Figure 9) a narrower shape ($\beta = 0.85$) than found experimentally ($\beta = 0.76$). This disparity becomes more pronounced for the orientation relaxation function (Figure 10), and it is attributed to an additional source of scattering due to internal degrees of freedom in the supramolecular assemblies. This additional contribution might affect the $I(q)$ in the high q range, but there is no obvious

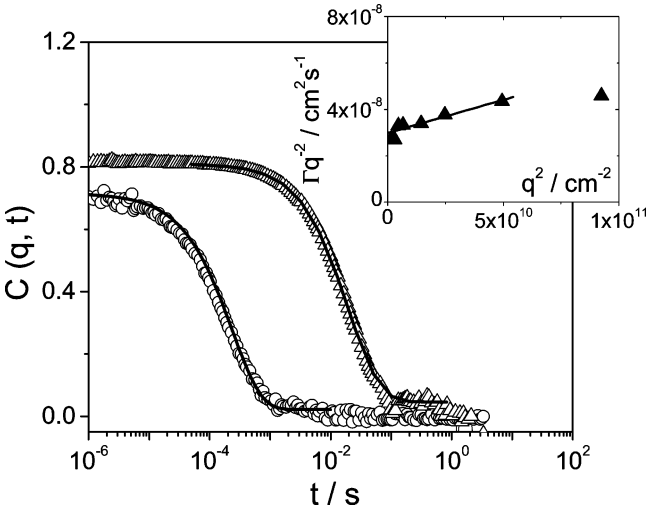

Figure 9. Relaxation functions $C(q,t)$ for the concentration fluctuations in 3.4×10^{-3} g/L PPPS-Ba21 for $q = 4.11 \times 10^{-3}$ nm^{-1} (Δ) and $q = 3.04 \times 10^{-2}$ nm^{-1} (O) at 20 °C. The solid lines denote representations according eq 9. The shape of the experimental $C(q,t)$ at high q is broader ($\beta = 0.76$) than the theoretical function ($\beta = 0.85$). The diffusion coefficient G/q^2 obtained from the experimental $C(q,t)$ is shown as a function of q^2 in the inset whereas the solid line denotes a linear dependence (eq 10).

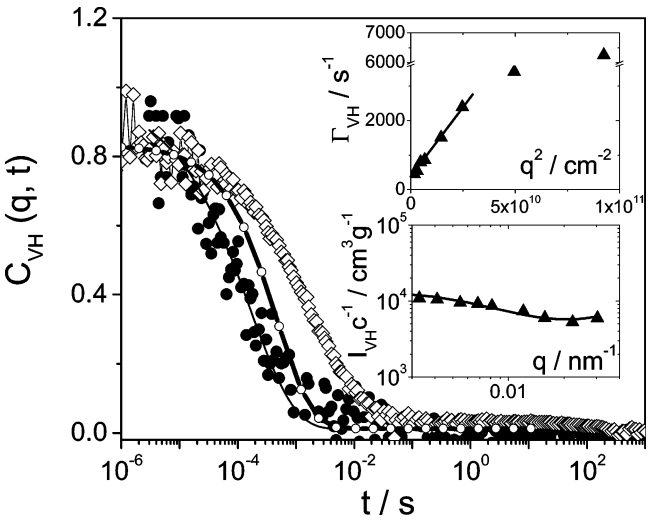

Figure 10. Orientation relaxation function $C_{or}(q,t)$ at $q = 4.11 \times 10^{-3}$ nm^{-1} (◇) and $q = 3.04 \times 10^{-2}$ nm^{-1} (●) for an aqueous solution of PPPS-Ba21 with $c_p = 3.4 \times 10^{-3}$ g/L at 20 °C. The dashed−dotted line denotes the calculated eq 14 with nonexponential parameter $\beta = 0.75$ function. The rate of the $C_{or}(q,t)$ and the time-averaged depolarized intensity $I_{VH}(q)$ are shown in the inset where the solid lines denote fits of eq 12 to the rate ($G_{VH}(q) = D_z q^2 + 6D_R$) and eq B1 (Appendix) to the intensity.

way to account for it. For large particles, the reduced first cumulant, Γ/q^2, shows a q dependence that can be written in the low q range limit as[32]

$$D_{app}(q) = \frac{\Gamma}{q^2} = D_z[1 + C(R_G{}^2 q^2) - ...] \quad (10)$$

where C is a dimensionless structure-sensitive parameter depending on the molecular architecture and polydispersity of the particles.[43]

The translational diffusion coefficient $D_z = 3 \times 10^{-8}$ cm^2 s^{-1} obtained from the intercept of the linear variation of Γ/q^2 (see inset to Figure 9) with q^2 is also a conformation index of the diffusing objects. For rigid rods[45] of length L_z and diameter d

$$D_z = \frac{k_B T}{3\pi\eta_0 L_z}\left(0.58 + \ln\left(\frac{L_z}{d}\right)\right) \quad (11)$$

where η_0 is the solvent viscosity. Using $d = 8$ nm, the experimental D_z leads to $\langle 1/L\rangle_z^{-1} = 725$ nm. For semiflexible chains with Kuhn segments length l_k, an alternative expression[34,46] can be also applied assuming a value for L_z as obtained from the static form factor $P(q)$ (Figure 8). In this case, l_k takes a value between 400 nm and L_z that again supports a rigid structure.

An additional evidence of these rigid structures originates from the measurable anisotropic light scattering. The main plot of Figure 10 displays the strong nonexponential $C_{or}(q,t)$ computed from the autocorrelation function (eq 1) of the depolarized light scattering intensity of PPPS-Ba21 at the same two extreme q values for comparison with the relaxation function $C(q,t)$ in Figure 9. The relaxation function for orientation fluctuations $C_{or}(q,t)$ decays via both translational and rotational motion, and hence for monodisperse rigid rods[45]

$$C_{or}(q,t) = I_{VH}(q)\exp[-(D_z q^2 + 6D_R)t] \quad (12)$$

where the relaxation rate $\Gamma_{VH}(q) = D_z q^2 + 6D_R$ yields the rotational diffusion

$$D_R = \frac{3k_B T}{\pi\eta_0 L^3}\ln\left(\frac{L}{d}\right) \quad (13)$$

at forward scattering ($q \to 0$). The q dependence of the amplitude $I_{VH}(q,L)$ in eq 12 is determined by the orientation correlations within the object with optical anisotropy $\langle\gamma^2\rangle = \beta_t^2(I_{VH}(q=0)/c)/(I_{VH,t}/r_t)(M_t/M_W)$ where the quantities with subscript t refer to the standard toluene with optical anisotropy β_t^2,molar mass M_t, and density ρ_t. The inclusion of the size polydispersity is possible for rigid rods for which the $C_{or}(q,t)$ (eq 12) is known. In analogy to eq 9, the function

$$C_{or}(q,t) = \frac{\int_0^\infty LW(L)\exp[-(D_z q^2 + 6D_R)t]\,dL}{\int_0^\infty LW(L)\,dL} \quad (14)$$

was employed to represent the experimental $C_{or}(q,t)$. At low q values, eq 14 with PD = 3 adequately describes the broad shape ($\beta \sim 0.75$) of the experimental orientation relaxation with a rate $G_{VH}(q)$ shown in the inset of Figure 10. Like the situation in $C(q,t)$ (Figure 9), eq 14 yields a too narrow ($\beta \sim 0.75$) shape compared to the experimental $C_{or}(q,t)$ (Figure 10) at the highest q, beyond the experimental error. We attribute this broader shape to additional orientation dynamics due to internal mobility of the anisotropic objects.

From the value of $D_R = 67\ s^{-1}$ (inset to Figure 10) and eq 13, we estimated $L = 660$ nm. Because of the large qL values, the $I_{VH}(q)$ displays a moderate but discernible q dependence, as shown in the lower inset of Figure 10; $I_{VH}(q)$ is distinctly different from the $P(q)$ (Figure 8) which supports its intrinsic nature free of artifacts at this low concentration. This important light scattering information is often lost due to the weak signal and precautions for a correct accessibility. In particular, there are only few experiments[47,48] to the best of our knowledge displaying a q-dependent $I_{VH}(q)$ in very dilute solutions. For long rigid rods ($qL \sim 1$), the analytical form[47] of $I_{VH}(q)$ (eq B.1 in the Appendix) modified to include polydispersity has been employed to match the experimental $I_{VH}(q)$ of Figure 10. The solid line denotes the theoretical prediction plus a baseline to account for the additional fast orientation fluctuations present at high q values. The value of the optical anisotropy $\langle\gamma^2\rangle$ of the aggregate consisting of ca. 10^5 benzene rings is about 10^9 times larger than the optical anisotropy of a single benzene ring (of toluene), and it suggests an enhancement of the optical anisotropy of the order of 10^5 owing to the intramolecular orientation correlations of the backbone phenylene rings.

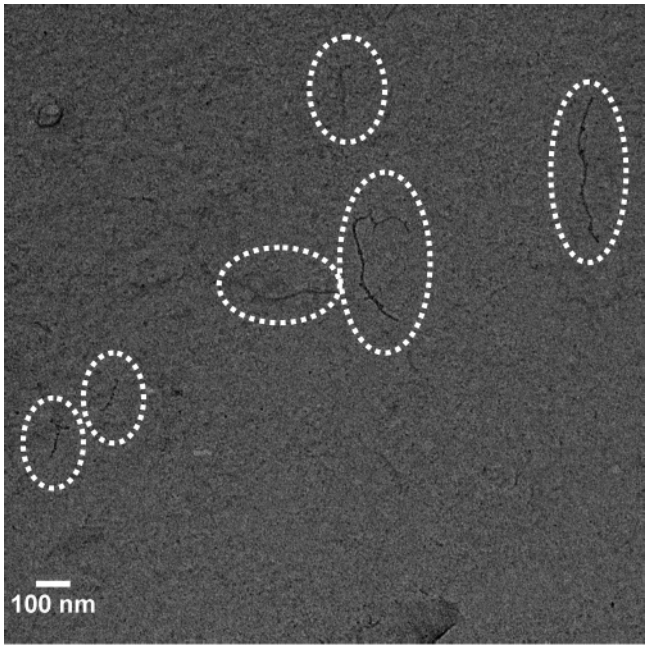

Figure 11. TEM micrograph (cryofixation method) of PPPS-Ba21 in aqueous solution at $c_p = 3.4 \times 10^{-3}$ g/L. Individual objects are encircled for better identification.

We do not wish to overemphasize by stating that the elucidation of the structure in PPPS-Ba21 is based on four different experimental quantities. Similar analysis was performed for the $P(q)$ of the other systems displayed in Figure 5 and the $C_{or}(q,t)$ in the presence of the divalent counterions. For the other two systems the shorter length and the increased flexibility renders the $C_{or}(q,t)$ very weak. Table 2 is a compilation of the structural properties of both the self-organized structures formed in the presence of calcium or barium ions.

Figure 11 displays a TEM image obtained from PPPS-Ba21 similar to Figure 4. Slender and elongated objects can be discerned which display a certain amount of curvature of the trajectory. A statistical analysis of many of such objects gave approximately $d = 8 \pm 1$ nm and $L = 447 \pm 22$ nm. The larger diameter compared to the objects seen in TEM micrographs of PPPS-H21 indicates an association as a consequence of the addition of divalent counterions as described above.

Conclusion

In this paper we present for the first time a detailed analysis of the self-organization of a conformationally rigid poly(*p*-phenylene)sulfonic acid regularly substituted with *n*-dodecyl side chains (see Figure 1 for the correct chemical formula). The starting polymer had a molar mass of $M_{W,p} = 21$ kg/mol, and it was studied under salt-free conditions; in other words, only hydrated protons serve as counterions in water as the solvent. As had been reported previously for the sodium salt of the same type of polymer, cylindrical micelles exist as the only object below a certain concentration, while above this concentration strong interactions between these micelles give aggregates of again rather well-defined size and shape in the submicron regime. They may be described as bundles of limited number

of individual micelles. At still higher concentrations a gel-like phase will be formed which exhibits signatures of liquid crystallinity.[28,30,31] Only the first two stages of self-organization have been looked at in detail in this work, namely the structure and dynamic of the cylindrical micelles in existence below the concentration of $c_p = 0.01$ g/L and of the clusters of micelles existing up to a concentration of $c_p = 0.01$ g/L. The micelles have a weight-average length of about 600 nm under salt-free conditions that is about 8 times the length of the individual constituent macromolecules. Their cross section contains about 14 such individual macromolecules aligned along the cylinder axis of the micelle. The shape of these micelles can be described by Koyama's form factor describing a weakly bending rod, that is, a wormlike object extending for only very few persistence lengths.

The important observation in this work is that addition of very small amounts of salt, like sodium chloride as example for a monovalent cation salt and calcium or barium chloride as examples for divalent cation salts, has a dramatic effect on the mode of self-organization of the polyelectrolyte. A detailed investigation by static and dynamic light scattering reveals that in the case of addition of NaCl to the solution of the micelles at a concentration which only exceeds the nominal concentration of the ionogenic sulfonic residues by a factor of 4; that is, at a concentration of $c_{salt} \sim 5 \times 10^{-5}$ mol/L, the number of polymer chains per cross section of the micelle increases by ca. 30% (19 chains) while the length of the micelle remains rather unchanged; however, the shape of the micelle remains still that of a weakly bending rod.

However, addition of 5×10^{-5} mol/L barium or calcium chloride induces a strong aggregation of the micelles to a new structure which is described as a bundle of a few micelles aggregated alongside and forming altogether a rodlike object. It can be described by the same form factor as the individual micelles. These objects have a very large mass of order of magnitude of 10^7 g/mol and are held together by attractive forces exerted by the ion cloud of divalent counterions close to the negatively charged surface of the micelles of the polymer. The weight-average length of these new bundle structures is of the same order of magnitude as that of the micelles found under salt-free conditions. Evidence of the existence of this structure comes from the strong optical anisotropy of the objects. These findings are qualitatively supported by direct imaging of the objects making use of cryofixation and mapping of the objects by TEM.

All these results point out how important it is to control the level of ionic impurities or purity of ionic additives in studies, which center around phenomena of self-organization in ionogenic polymers whether synthetic as in this article or biogenic. Very small amounts of salt that can be easily introduced in the course of preparation of the material or may be contained in the form of traces in the water used as solvent can have dramatic effects on the size and form of aggregates which are formed from the constituent macromolecules. Finally, few theoretical attempts to rationalize the well-defined structures in the presence of monovalent counterion have already been reported.[40,42,49−52]

Acknowledgment. We thank Prof. Dr. M. Schmidt (University of Mainz) for suggesting us the Koyama form factor and Dr. E. van Ruymbeke (FO.R.T.H.) for the assistance in some computations. For the TEM micrographs, we are grateful to Dr. I. Lieberwirth (Max Planck Institute for Polymer Research Mainz).

Appendix

A. Definition of Koyama's form factor:[36−39]

$$P_{\text{Koyama}}(L_r, ql_k) = \frac{2}{L_r^2}\int_0^{L_r}(L_r - x)\exp\left[-\frac{1}{3}s^2 xf(x)\right]\frac{\sin(sxg(x))}{sxg(x)}\,dx \quad \text{(A.1)}$$

with l_k the statistical Kuhn segment length, μ the inverse of l_k, $\mu = (1/l_k)$, L the contour length, s the reduced q, $s = (q/2\mu)$, L_r the reduced contour length, $L_r = 2\mu L$, t the reduced Kuhn segment length, $t = (x/2\mu)$, x the number of segments per reduced length t, $\langle r^2\rangle$ the second moment of the end-to-end distribution function, and $\langle r^4\rangle$ the fourth moment of the end-to-end distribution function, with

$$K = \frac{\langle r^4\rangle}{\langle r^2\rangle^2} \quad \text{(A.2)}$$

$$\langle r^2\rangle = \frac{1}{\mu}\left(t - \frac{1}{2\mu}(1 - e^{-2\mu t})\right) \quad \text{(A.3)}$$

$$\langle r^4\rangle = \frac{1}{\mu^2}\left(\frac{5t^2}{3} - \frac{26t}{9\mu} - \frac{1}{54\mu^2}(1 - e^{-6\mu t}) + \frac{2}{\mu^2}(1 - e^{-2\mu t}) - \frac{t}{\mu}e^{-2\mu t}\right) \quad \text{(A.4)}$$

$$xf(x) = \frac{(2\mu)^2}{2}\langle r^2\rangle\left(1 - \frac{\sqrt{10}}{2}\sqrt{1 - \frac{3K}{5}}\right) \quad \text{(A.5)}$$

$$x^2g^2(x) = \frac{1}{2}(2\mu)^2\langle r^2\rangle\left(\sqrt{\frac{5}{2}}\sqrt{1 - \frac{3K}{5}}\right) \quad \text{(A.6)}$$

$$xg(x) = \sqrt{x^2g^2(x)} \quad \text{(A.7)}$$

B. VH form factor for rigid rod[47]

$$P = \frac{\int_0^\infty c4W(L)L\,dL}{\int_0^\infty W(L)L\,dL} \quad \text{(B.1)}$$

with $x = qL$ and

$$c1 = \frac{\cos 2x}{2x^2} + \frac{\sin 2x}{4x^3} - \frac{1}{x^2} + \frac{Si(2x)}{x} - \frac{3}{4}\left(\frac{\sin 2x}{8x^5} - \frac{\cos 2x}{4x^4} + \frac{\sin 2x}{4x^3} + \frac{\cos 2x}{2x^2} - \frac{4}{3x^2} + \frac{Si(2x)}{x}\right) \quad \text{(B.2)}$$

$$c2 = \frac{5\sin 2x}{8x^5} - \frac{5\cos 2x}{4x^4} + \frac{\sin 2x}{4x^3} + \frac{\cos 2x}{2x^2} - \frac{8}{3x^2} + \frac{Si(2x)}{x} \quad \text{(B.3)}$$

with

$$Si(x) = \int_0^x \frac{\sin z}{z}\,dz$$

$$c3 = -\frac{\cos\theta}{4} \quad \text{(B.4)}$$

$$c4 = \frac{9k}{4}(c1 + c2c3) \tag{B.5}$$

and

$$W(L) = \frac{L^m}{m!} y^{m+1} e^{-yL} \tag{B.6}$$

where

$$y = \frac{m+1}{L_W} \tag{B.7}$$

and

$$m = \frac{1}{PD - 1} \tag{B.8}$$

References and Notes

(1) Barrat, J.-L.; Joanny, J. F. *Adv. Chem. Phys.* **1996**, *94*, 1.
(2) Schmitz, K. S. *Macroions in Solution and Colloidal Suspension*; VCH Publishers: New York, 1993.
(3) Förster, S.; Schmidt, M. *Adv. Polym. Sci.* **1995**, *120*, 51.
(4) Holm, C.; Joanny, J. F.; Kremer, K.; Netz, R. R.; Reineker, P.; Seidel, C.; Vilgis, T. A.; Winkler, R. G. *Adv. Polym. Sci.* **2004**, *166*, 67.
(5) Hara, M., Ed. *Polyelectrolytes: Science and Technology*; Marcel Dekker: New York, 1993.
(6) Holm, C., Kekicheff, P., Podgornik, R., Eds. *Electrostatic Effects in Soft Matter and Biophysics*; Kluver Academic Publishers: Dordrecht, 2001.
(7) Eigen, M.; Schuster, P. *The Hypercycle−A Principle of Nature Self-Organisation*; Springer: Heidelberg, 1979.
(8) Eigen, M.; Schuster, P. *J. Mol. Evol.* **1982**, *19*, 47.
(9) Anderson, P. W.; Stein, D. L. In *Self-Organizing Systems*; Yates, I., Eugene, F., Eds.; Plenum Press: New York, 1987.
(10) Saenger, W. *Principles of Nucleic Acid Structure*; Springer: Heidelberg, 1984.
(11) Kjellen, L.; Lindahl, U. *Annu. Rev. Biochem.* **1991**, *60*, 443−75.
(12) Darnell, J.; Lodish, H.; Baltimore, D. *Molecular Cell Biology*; Scientific American Books, Inc.: New York, 1990.
(13) Branden, C.; Tooze, J. *Introduction to Protein Structure*; Garland: New York, 1997.
(14) Creighton, T. E. *Proteins: Structures and Molecular Principles*; Freeman: New York, 1992.
(15) Alberts, B.; Bray, D.; Lewis, J.; Raff, M.; Roberts, K.; Watson, J. D. *Molecular Biology of the Cell*; Garland: New York, 1989.
(16) Manning, G. S. *J. Chem. Phys.* **1969**, *51*, 924, 3252.
(17) Schiessel, H.; Pincus, P. *Macromolecules* **1998**, *31*, 7953.
(18) Limbach, H. J.; Holm, C. *J. Phys. Chem. B* **2003**, *107*, 8041.
(19) Oosawa, F. *Polyelectrolytes*; Marcel Dekker: New York, 1971.
(20) Holm, C.; Rehan, M.; Oppermann, W.; Ballauff, M. *Adv. Polym. Sci.* **2004**, *166*, 1.
(21) Ise, N.; Sogami, I. S. *Structure Formation in Solution: Ionic Polymers and Colloidal Particles*; Springer: Heidelberg, 2005.
(22) Noda, I., Kokufuta, E., Eds. *Polyelectrolytes*; Yamady Sci. Foundation: Osaka, 1999.
(23) Rulkens, R.; Wegner, G.; Enkelmann, V.; Schulze, M. *Ber. Bunsen-Ges. Phys. Chem.* **1996**, *100*, 707.
(24) Bockstaller, M.; Köhler, W.; Wegner, G.; Vlassopoulos, D.; Fytas, G. *Macromolecules* **2000**, *33*, 3951.
(25) Bockstaller, M.; Köhler, W.; Wegner, G.; Vlassopoulos, D.; Fytas, G. *Macromolecules* **2001**, *34*, 6353, 6359.
(26) Kötz, J.; Kosmella, S.; Beitz, T. *Prog. Polym. Sci.* **2001**, *26*, 1199.
(27) Rulkens, R.; Wegner, G.; Thurn-Albrecht, T. *Langmuir* **1999**, *15*, 4022.
(28) Zaroslov, Yu. D.; Gordelily, V. I.; Kuklin, A. I.; Islamov, A. H.; Philippova, O. E.; Khokhlov, A. R.; Wegner, G. *Macromolecules* **2002**, *35*, 4466.
(29) Belack, J. Ph.D. Thesis, Johannes-Gutenberg-Universität, Mainz, 2000.
(30) Rulkens, R.; Schulze, M.; Wegner, G. *Macromol. Rapid Commun.* **1994**, *15*, 669.
(31) Thurmond, D. *J. Polym. Sci.* **1952**, *8*, 607.
(32) Brown, W., Ed. *Dynamic Light Scattering*; Clarendon Press: Oxford, 1993.
(33) Provencher, S. W. *Comput. Phys. Commun.* **1982**, *27*, 229.
(34) Kratochvil, P. *Classical Light Scattering from Polymer Solutions*; Elsevier: Amsterdam, 1987.
(35) Becker, A.; Köhler, W.; Müller, B. *Ber. Bunsen-Ges. Phys. Chem.* **1995**, *99*, 600.
(36) Koyama, R. J. *J. Phys. Soc. Jpn.* **1973**, *34*, 1029.
(37) Schmidt, M.; Paradosi, G.; Burchard, W. *Macromol. Chem., Rapid Commun.* **1985**, *6*, 767.
(38) Lang, P.; Kajiwara, K.; Burchard, W. *Macromolecules* **1993**, *26*, 3992.
(39) Pötschke, D.; Hickl, P.; Ballauf, M.; Astrand, P.-O.; Pedersen, J. S. *Macromol. Theory Simul.* **2000**, *9*, 345.
(40) Prabhu, V. M.; Muthukumar, M.; Wignall, G. D.; Melnichenko, Y. B. *J. Chem. Phys.* **2003**, *119*, 4095.
(41) Fütterer, T.; Hellwig, T.; Findenegg, G. H.; Frahn, J.; Schlüter, A. D. *Macromolecules* **2005**, *38*, 7443, 7451.
(42) Olvera de la Cruz, M.; Belloni, L.; Delsanti, M.; Dalbiez, J. P.; Spalla, O.; Drifford, M. *J. Chem. Phys.* **1995**, *103*, 5781.
(43) Schmidt, M. *Macromolecules* **1984**, *17*, 553.
(44) Higgins, J.; Benoit, H. *Polymers and Neutron Scattering*; Oxford University Press: Oxford, 1996.
(45) Zero, K.; Pecora, R. Dynamic Depolarized Light Scattering. In *Dynamic Light Scattering*; Pecora, R., Ed.; Plenum Press: New York, 1985.
(46) Yamakawa, H.; Fujii, M. *Macromolecules* **1973**, *3*, 407.
(47) Horn, P.; Benoit, H.; Oster, G. *J. Chim. Phys.* **1951**, *48*, 1.
(48) Somma, E.; Loppinet, B.; Fytas, G.; Setayesh, S.; Jacob, J.; Grimsdale, A. C.; Muellen, K. *Colloid Polym. Sci.* **2004**, *282*, 867.
(49) Potemkin, I. I.; Khokhlov, A. R. *J. Chem. Phys.* **2004**, *120*, 10848.
(50) Potemkin, I. I.; Oskolkov, N. N.; Khokhlov, A. R.; Reineker, P. *Phys. Rev. E* **2005**, *72*, 021804.
(51) Limbach, H. J.; Holm, C.; Kremer, K. *Macromol. Chem. Phys.* **2005**, *206*, 77.
(52) Limbach, H. J.; Sayar, M.; Holm, C. *J. Phys.: Condens. Matter* **2004**, *16*, 2135.

MA061228V